

Nanoscale

Accepted Manuscript



This is an *Accepted Manuscript*, which has been through the Royal Society of Chemistry peer review process and has been accepted for publication.

Accepted Manuscripts are published online shortly after acceptance, before technical editing, formatting and proof reading. Using this free service, authors can make their results available to the community, in citable form, before we publish the edited article. We will replace this *Accepted Manuscript* with the edited and formatted *Advance Article* as soon as it is available.

You can find more information about *Accepted Manuscripts* in the [Information for Authors](#).

Please note that technical editing may introduce minor changes to the text and/or graphics, which may alter content. The journal's standard [Terms & Conditions](#) and the [Ethical guidelines](#) still apply. In no event shall the Royal Society of Chemistry be held responsible for any errors or omissions in this *Accepted Manuscript* or any consequences arising from the use of any information it contains.

Formation of Hollow Silica Nanospheres by Reverse Microemulsion

Chen-Han Lin,^a † Jen-Hsuan Chang,^a † Yi-Qi Yeh,^b Si-Han Wu,^a Yi-Hsin Liu,^a and
Chung-Yuan Mou^{a*}

^a Center for Condensed Matter Sciences, and Department of Chemistry, National
Taiwan University, Taipei, Taiwan 10617

^b National Synchrotron Radiation Research Center, Hsinchu, Taiwan 30076

† Equal contribution

* Corresponding author: cymou@ntu.edu.tw

KEYWORDS reverse microemulsion, silica, nanoparticles, hollow, SAXS.

ABSTRACT: Uniform hollow silica nanospheres (HSNs) synthesized with reverse microemulsion have great application potential as nanoreactors since enzyme or nanocatalysts can be easily encapsulated de-novo in synthesis. Reverse microemulsions (w/o type) comprising of polymeric surfactant Polyoxyethylene (5) isooctylphenyl ether (Igepal CA-520), ammonia and water in a continuous oil phase (alkanes) coalesce into size-tunable silica nanoparticles via diffusion aggregation after introduction of silica precursors. Here we elucidate in details the growth mechanism for silica nanoparticles via nucleation of ammonium-catalyzed silica oligomers from tetraethylorthosilicate (TEOS) and aminopropyltrimethoxy silanenano porous (APTS) in the reverse microemulsion system. The formation pathway was studied in-situ with small angle X-ray scattering (SAXS). We find a four-stage process showing a sigmoidal growth behavior in time with a crossover from induction period, early-stage of nucleation, coalescence growth and a final slow-down of the growth. Various characterizations (TEM, N₂ isotherm, dynamic light scattering, zeta potential, NMR, elemental analysis) reveal diameters, scattering length density (SLD), mesoporosity, surface potentials and chemical compositions of the HSNs. Oil phases of alkanes with different alkyl chains are systematically employed to tune the sizes of HSNs by varying oil molar volumes, co-solvent amounts or surfactant mixture ratios. Silica condensation is incomplete in the core region with silica source of TEOS and APTS leading to hollow silica nanosphere after etching with warm water.

Introduction

Recently, hollow silica nanospheres (HSNs) are receiving increased attention from researchers. Hollow silica nanoparticle with a nanoporous shell is a valuable material for its possible functions as nanoreactor¹ in catalysis or nanocarrier² in drug delivery. Nanoporous silica shell has advantages in its chemical stability, optical transparency, porous structure, and selective permeability. As a nanoreactor, it can encapsulate catalytic agent such as semiconductor nanoparticle,³ kegging ions,⁴ gold nanoparticle⁵,⁶ or enzyme.^{7, 8} The porous shell could be designed as a short conduit for reactant/product while selectively keeping poisons outside.^{5, 6} As a carrier in nanomedicine, its easy functionalization¹ on the external surface and encapsulated payloads inside can be exploited to build multifunctionality^{9, 10} such as carrying drug, enzyme, contrast agent and cell recognition ligands. Its potential in both fields is rich.

In their applications, precise synthetic control of the silica nanospheres, including diameter, porosity, and encapsulation, would be valuable in its future developments. Present methods of making hollow silica sphere include templating silica sol-gel synthesis with sacrificial solid nanospheres,¹¹ emulsion droplets,^{12, 13} or vesicular structures.¹⁴⁻¹⁶ However, the sizes of the HSNs in most of the reports are above 200 nm in diameter as in emulsion or vesicle templating. Such large size is usually not effective for biomedical applications since cell uptake is limited. Recently, there are a few reports giving sub-100 nm size. Hollow silica nanospheres around 30-60 nm have been made with catanionic vesicles as template.¹⁷ Williamson et al. reported a synthesis of porous hollow silica nanostructures using hydroxyapatite nanoparticle templates.¹⁸ However, most of the reports did not show deliberate size control.

Microemulsion is a thermodynamic equilibrium system; its droplet size is thus typically uniform.¹⁹ In principle, one can systematically control its size by changing the interfacial curvature through surfactant/co-surfactant composition or solution conditions.^{20, 21} With sol-gel silica condensation in the microemulsion droplets, stable solid silica nanoparticles have been synthesized, in both w/o (water-in-oil) type²²⁻²⁵ or o/w type microemulsion.²⁶ In the two types of microemulsion, w/o type reverse microemulsion works better as template when tetraethylorthosilicate (TEOS) is used as silica source because other undesirable surfactant/silicate organizations (such as mesocellular foam) can be avoided in oil-continuous phase.²⁷ In fact, w/o type microemulsion method has been used in making solid silica nanoparticle^{24, 25, 28-30} or silica-coating of pre-made inorganic nanoparticles.^{31, 32}

HSN has been synthesized by limited sol-gel condensation with w/o microemulsion such that the incompletely condensed core can be etched away in alkaline condition.^{9, 10, 33-35} Previously, we reported a synthesis of hollow silica nanosphere by a two-step process³: First, we make a Stöber-like synthesis of solid silica nanoparticle (SSN) within a reverse microemulsion (w/o) system of alkane, water, block copolymer amphiphiles, co-surfactant (hexanol), TEOS and aminopropyltrimethoxysilane (APTS). Second, an etching step in synthesizing HSN was employed to remove the core portion of silica nanoparticles. The resulting hollow silica nanospheres (HSNs) have several desirable features: (1) cargos such as nanoparticles of gold or iron oxide³⁻⁶ or enzyme molecules^{8, 36} can be easily encapsulated in the cavity of HSN. (2) The porous silica shell could function as a selective screen keeping out poisons while allowing small substrates for the catalysis.⁵ The approach is especially suitable for

encapsulating fragile substance such as enzyme in the water-pool of W/O microemulsion. The de-novo enzyme encapsulation in microemulsion templating solved nicely the ship-in-bottle synthesis problem.^{8, 36, 37} In most of other approaches of making hollow metal oxides, such as in solid replacement methods,^{38, 39} post-synthesis loading into cavity would be limited.

For the increasingly important hollow silica nanosphere, there has been little systemic study on its formation mechanism and size control. It would be desirable to perform a systematic investigation of the reverse microemulsion templating method to understand its formation mechanism. Zhao and coworkers have studied systematically the control of the size of solid silica nanoparticles by varying the organic solvents used in a w/o microemulsion alkaline synthesis.⁴⁰ Evolution of reverse microemulsion-TEOS systems in the synthesis of silica nanoparticles has also been followed.⁴¹⁻⁴⁴ However, there has been little mechanistic study for the hollow silica nanospheres. In this work, we study the effects of varying hydrocarbon solvents, alcoholic co-surfactant and compositions of a mixed surfactant system on the size of the hollow silica product. We then rationalize the results by evoking molecular model of surfactant packing for the interface of microemulsion.⁴⁵

To understand the evolution of the nanostructures in the process of synthesis, we performed *in-situ* SAXS measurements, a powerful technique for studying the evolution of size and density (contrast) of the nanoparticle in microemulsion^{42, 44, 46, 47} We analyze time-resolved scattering patterns with a nanosphere model to understand their time evolution behaviors. Simulations of the patterns allow us to deduce the changes of both diameter and scattering lengths density. We employ a mild etching

process that removes silica oligomers in the cores to produce well-defined hollow nanostructures.^{48, 49} The compositional changes were evaluated by elemental analysis and NMR. Combining the results in synthesis controls of sizes of HSN and in situ SAXS, and dynamical light scattering, we finally discuss the growth of HSN in terms of a proposed formation mechanism.

2. Experimental Section

Materials sources and purity are described in supporting information. Here we give experimental procedures for synthesis and characterizations.

2.1 Synthesis of hollow silica nanospheres (HSNs): The hollow silica nanospheres were synthesized in water-in-oil (w/o) reverse microemulsion system. First, 29.65g of cyclohexane, 3.26 mL CA-520 and 700 μ L deionized water were mixed together and stirred at room temperature, in order to generate the reverse microemulsion system. Then, 200 μ L of TEOS and 50 μ L of ethanol solution of APTS were added into mixture. The ethanolic APTS solution was prepared by adding 200 μ L of APTS to 1.4 mL of absolute ethanol. Two hours later, 500 μ L of ammonia hydroxide (28-30 wt %) was added to initiate the hydrolysis of TEOS and APTS. The hydrolysis and condensation process was kept at 20 °C in all synthesis of HSN and SAXS, MAS-NMR and dynamical light scattering experiments. The as-synthesized nanospheres were separated from solution by centrifugation at 15000 rpm for 15 min and washed with ethanol twice to remove the surfactant. Afterwards, the solid nanospheres were stirred in warm water for transforming into hollow silica nanospheres (HSNs). Again, the

silica hollow nanospheres were separated from solution by centrifugation and then dried at room temperature.

2.2 Synthesis of HSNs by changing the solvent of the reverse microemulsion system:

Various amounts of solvents, 29.65 g of cyclohexane, 30.29 g of *n*-hexane, 40.24 g of *n*-octane, 50.1 g of *n*-decane, 60.0 g of *n*-dodecane were used in order to fix molar ratio of system. In order to obtain a clear solution, 2.5 mL of *n*-hexanol was added into the solutions. The rest of work-up procedure is the same as in 2.1.

2.3 Synthesis of HSNs by changing the ratio of CA-520 and Triton X-100:

14.83g of cyclohexane were mixed with various amounts of CA-520 (3.26, 2.45, 1.63, 0.82 and 0 mL) and Triton X-100 (0, 1.25, 2.5, 3.75, and 5 g). 0~4 mL of *n*-hexanol as co-surfactant was added into the mixture of various ratio of CA-520 to Triton X-100. 350 μL of H_2O was added into the solution to form a clear solution. 100 μL of TEOS and 25 μL of ethanolic solution of APTS were added into the mixture, and then 250 μL of aqueous ammonia (28~30 wt %) was added into solution after 2 hours. The rest of the procedure is the same as in 2.1.

2.4 Synthesis of HSNs by varying the volume of *n*-hexanol:

The reverse microemulsion system was made by 14.83 g of cyclohexane, 5 g of Triton X-100, 350 μL of deionized water, and the different volume of *n*-hexanol (1, 3, 5, and 7 mL). It was noticed that the solution was turbid all the time, rather than a clear solution. Then, 100 μL of TEOS and 25 μL of APTS ethanolic solution were added to the mixture under continuously stirring. After 2 hours, 250 μL of aqueous ammonia (28-30 wt %) was added to the mixture to initiate the hydrolysis of silanes, and the mixture was stirred for 36 hours at 20 °C. The as-synthesized solid silica nanospheres were isolated by

adding 95% ethanol to destabilize the microemulsion system and then by centrifugation. The rest of procedure is the same as **2.1**.

2.5 Small-angle X-ray scattering (SAXS) measurements: The SAXS measurements were conducted at the BL23A SWAXS end station in National Synchrotron Radiation Research Center (NSRRC, Taiwan). With 12 keV synchrotron X-rays (wavelength = 1.034 Å) and a sample-to-detector distance of 3.8 m, the scattering wavevector q , defined as $4\pi\lambda/\sin\theta$ with scattering angle 2θ , covered from 0.005 Å⁻¹ to 0.2 Å⁻¹. The *in situ* formation process of SSN was performed in a flow-cell system, as depicted in Figure SI-2. We use small-angle X-ray scattering (SAXS) technique to elucidate the morphology evolution process for silica nanoparticles. During the growth period, a solution composed of cyclohexane, CA-520, TEOS and APTS were circulated between the reaction flask and a Kapton-sealed stainless cell by a rotary pump, with a temperature controlled in a cold water bath (20°C) (Fig. S2). Consecutive SAXS scans (Fig. 3 and Fig. S3) with a short exposure time (30 s) were collected at various time after TEOS/APTS hydrolysis was initiated by ammonium hydroxide. Data were corrected for electronic noise, sample transmission, and detector sensitivity, followed by a scaling to absolute intensity $I(q)$ in units of cm⁻¹ via scattering from water. More details for analysis of SAXS data can be found in Supporting Information.

3. Results

3.1 Synthesis and characterization: Our synthesis was conducted in a reverse microemulsion system of water-oil-surfactant with alkanes as continuous phase, water as dispersed phase, and neutral surfactant Igepal CA-520 (polyoxyethylene (5) iso-

octylphenyl ether) as a surface-active agent. For detailed study of mechanistic, we focus primarily on using cyclohexane as oil phase. Initially, the surfactant was dissolved in cyclohexane to form a clear solution. When a small amount of water (700 μL) was introduced, the solution turned to turbid for a short period of time and then became clear. This indicates that a reverse microemulsion system was formed with nano-sized water droplets dispersed in the oil phase. Two silica precursors, TEOS and APTS, were initially dispersed in the oil phase and gradually hydrolyzed in the water droplet upon ammonia addition. Subsequent silica condensation, resulting in formation of silica nanoparticles, occurred in the water phase. Representative TEM image (Fig. 1a) indicates formation of solid silica nanoparticles (SSNs) with uniform final particle sizes of 30 ± 3 nm. The solid nanoparticles were transformed to hollow silica nanospheres (HSNs), by washing with a warm ethanol-water solution (40-50 $^{\circ}\text{C}$). During the washing, silicate oligomers (in the core) and some of the amphiphiles (on the shell) are extracted. There is little size reduction or shape deformation in the etching process as evidenced by the TEM images of SSNs and HSNs (Fig. 1c,d). For the cyclohexane system, the final dried HSNs show an average diameter of 29 nm and a shell thickness around 5 nm (Fig. 1b).

The N_2 adsorption-desorption isotherm (Fig. 2) shows a peculiar texture (the hysteresis loop), different from the amorphous silica of nanoparticles obtained by Stöber synthesis⁵⁰. This is due to the nanopores on the shells of HSNs. The surface area and pore volume of the calcined HSNs at 359.14 $\text{m}^2 \text{g}^{-1}$ and 1.09 $\text{cm}^3 \text{g}^{-1}$ which are not greatly bigger than those of as-washed HSNs (170.74 $\text{m}^2 \text{g}^{-1}$ and 0.72 $\text{cm}^3 \text{g}^{-1}$). (Table 1) The large surface areas are partly attributed to the mesopores on the shells

that were initially occupied by CA-520 but later removed by extraction and further by calcination. The micropores (less than 1 nm) in HSN and calcined HSN are responsible for substantial fraction of the total area. In SSN, the pores are completely microporous in nature. These micropores (less than 1 nm) are the results of stacking of very small nanoparticles which are also present in Stöber silica. After washing to create the hollow voids, some pores are already created in extraction to connect the outer and inner voids and thus there is not significant difference in pore volume between as-washed and calcined HSNs. After calcination, the hysteresis loops in the isotherm increases and shifts to lower pressure regimes (Fig. 2b, $0.45 < p < 0.8$), indicating resulting in smaller pores on the HSN particles. In comparison, the surface area and pore volume for unwashed SSN are much smaller. (Table 1) Zeta potential measurements were measured on the as-etched HSNs in a titration pH range between 3 and 10 (Fig. S1.) Isoelectric point of the HSNs is determined at pH= 5.2 which is significantly higher than those of amorphous silica (around pH= 2-3). The higher isoelectric point is due to the functionalized amine group in the HSNs. Below the isoelectric point (pH < 5), HSN becomes positively charged due to protonation of amines in APTS. Above the isoelectric point (pH > 6), the HSNs are negatively charged due to de-protonation of surface silanols groups.

3.2 Time Evolution by SAXS Study: Initial examination of the SAXS profile in Figure 3a indicates a growth of polydisperse distribution of nanospherical domains as time increases. Except for the two initial time data which can be fitted by unimodal size distribution of nanospheres, all the SAXS data for the rest of the time were fitted by bimodal distribution of sizes of various SLD. Four selected fittings of SAXS

profiles are shown in Fig. 3 b-e. At initial time, the low q part of SAXS spectra did not indicate any particle of size bigger than 15 nm. Thus, we fit SAXS spectra with unimodal distribution of spheres of diameter less than 15 nm. Compared to SAXS of collected and dried SSN (Figure 3e), the less oscillation at intermediate q ($\sim 0.02 \text{ \AA}^{-1}$) in Fig. 3e hints there are population of small nanostructure around ~ 10 nm coexisting with the silica nanospheres in solution, thus smearing out the SAXS oscillations.

Before silica condensation, the microemulsion shows a water droplet size of 8 nm. From the IGOR fitting analysis, nanoparticles with increasing SLD values and growing sizes were identified after the addition of ammonia solution. The nanoparticles with larger SLD values can be directly evidenced in TEM images (Fig. S4) which indicate the growth of silica nanoparticle evolving from a size similar to the microemulsion droplet (7-8 nm). Within the first hour of initiation, a quick reduction in SAXS intensities indicates a consumption of microemulsion droplet population and a small growth of particle sizes (~ 10 nm) (Fig. 4b). At about the same time, the fitted SLD (Fig. 4a) shows a rapid increase with time suggesting a rapid hydrolysis of TEOS and APTS and nucleation within the w/o droplet. We also see a very large fluctuation of the size of nanoparticles at about 100 min which is characteristic of a period of rapid nucleation burst.⁵¹ After 100 min, the total scattering intensity at low q gradually increased giving a continuous increase of size of the silica nanoparticles while its SLD remains roughly constant until 600 min. In this period, the continuous growth of size of silica nanoparticle is driven by coalescence of hydrolyzed TEOS and APTS inside the microemulsion droplet. The medium- q scattering profile ($0.006 < q < 0.1$) is mainly due to increasing sizes and SLD values of the growing nanoparticles whereas

the high- q scattering profile ($q > 0.1$) yields sizes and SLD values for those of the initial microemulsion droplets. The SAXS and fitting results from the medium- and high- q regime can provide us a picture in evolutions of diameters and SLD values as well as aggregative behaviors during the growth process. We observed a bi-modal distribution of spherical nanoparticles. The smaller ones of 8 nm size with low and unchanging SLD are the water droplets in microemulsion. Apparently those are the un-nucleated droplets with mainly water inside. The large growing spheres are the sites of sink for coagulation driven by silica condensation. The coagulation behaviors of nanoparticles suggest a coalescence pathway for the final solid silica nanoparticles (SSNs). Diameter distributions and the SLD values can be derived from polydispersity (ρ) and its fitted diameter (d);

We plotted growth parameters (SLD and diameter) of the SSNs with individual variance bars as shown in Figure 4a and 4b. In the earliest stage (< 30 min), the variance for the diameters and SLD values were relatively small with a nearly constant diameter size (~ 8 nm) and SLD ($9.5\text{-}9.7 \times 10^{-6} \text{ \AA}^{-2}$) for the microemulsion comprising water only. After 1.5 h (90 min), SAXS profiles suggest increased polydispersities (~ 0.3 in Fig. 4a) that coincide with an observation of wide diameter distributions in TEM analysis (Fig. S3). This phenomenon suggests that the initial nucleation of SSNs results in big diameter fluctuations with higher polydispersity. In the next few hours, the SSNs grew to be larger than 30 nm and SLD values increased to 1.23×10^{-5} whereas the SLD values for pure H_2O and silica are known to be 9.46×10^{-6} and $1.8 \times 10^{-5} \text{ \AA}^{-2}$ respectively.⁵² The SLD contrasts between H_2O and silica suggest that SSNs are low-density soft silica matrix comprising of mainly H_2O , ethanol and some

partially condensed silica from which less condensed silicates may be removed by washing with warm water. In the period 1.5 to 10 hours (metastable zone), the SLD values reached the first plateau stages by absorbing hydrolyzed polymeric silica inside the microemulsion water droplets. In the next 10-18 hours, the silica nanoparticles became matured with a small increase of SLD. Apparently, water were further consumed in silica condensation and one see a small further increase of SLD. The final SLD value ($1.3 \times 10^{-5} \text{ \AA}^{-2}$) never reaches the high value for pure silica ($1.8 \times 10^{-5} \text{ \AA}^{-2}$). Thus the final SSNs collected by centrifugation still contain substantial amount of uncondensed silanol and thus removable by washing. In Fig. 4b, we also plotted the final size of collected SSNs as measured by TEM (red curve). Since, in the SSNs are collected after precipitation, centrifuge and drying, excess water and alcohols in the droplet pools have been removed. Thus, it is expected the size of SSNs determined by TEM should be smaller than the size of water droplet in reverse microemulsion.

In order to understand better the growth mechanism of the silica nanoparticle in solution, we re-plotted the time evolution of its diameter in a log-log graph as shown in Fig. 4c. One can see clearly the evolution can be divided into stages. We discuss the growth mechanism in greater details based on this plot in discussion section after the rest of experimental data in this section are presented.

3.3 Etching to form hollow nanospheres: After the nanoparticles (SSNs) were made, they were etched in warm water to make hollow nanospheres (HSNs) with interior hollow cavity and nanoporous silica shells. Fig. 5 shows the time evolution of the etching process. The initial SSN was quite uniform in size. Initial etching at 10 min washing shows many isolated small voids inside SSNs. At 20 min, we obtained hollow

center voids with some residue silica inside.(Fig. 5c) Finally, at 40 min, well-etched HSNs were obtained showing the same size as the original SSNs. Elemental analysis and ^{29}Si NMR can monitor TEOS and APTS condensation and etching-release degrees during the process. The ~ 5 nm thick shells in HSNs contains twice amounts of the nitrogen element(from APTS) as that in the SSNs while the supernant solution from etching process contains only small amounts of nitrogen (Table S1). According to the C, H, N elemental analysis (Table S1) and mass-transfer calculations of APTS, TEOS, CA-520 and SiO_2 (Table S2) show HSN shells receive 35.8% of TEOS-derivatives and 76.1% of APTS-derivatives from the SSNs prior to the etching process. The washed out content was mainly water and TEOS-derivatives (64.2 %) with minor quantity of APTS (23.9 %). To further investigate the siloxane species in as-synthesized silica, solid state ^{29}Si NMR spectroscopy was employed to evaluate degrees of condensation before and after the etching procedure. In Figure 6a, one observed a significant reduction of Qx species while the T species due to APTS remain about the same level (Fig. 5a, red to blue curves). This confirms the fact that TEOS-derivatives were the dominant leached species from HSN cores. After deconvolution of Gaussian profiles, slightly increasing Q^3 , and Q^4 and decreasing Q^2 intensities (Fig. 6b and 6c and Table S3) indicate condensation continued to occur during the etching process.

Also in the etching process, the ethanol-washing step is to remove the surfactant CA-520. It not only removed the surfactants on the external surface but also created some pores by removing the pore-templating surfactant. In the next warm-water washing step, the uncondensed species inside SSN(mainly from TEOS) were leached out through the pores on the shell. In summary, the etching process in a warm solution

successively release mainly TEOS- and in minor APTS-derivatives into the solution. The synthesis of HSNs depends critically on incorporating APTS which leads to partial condensation and removal of TEOS in the facile washing process.^{9, 10}

3.4 Growth Mechanism: Here we propose a mechanism of formation of the uniform hollow silica nanospheres in the w/o microemulsion. The reverse microemulsion served as soft container to initiate the nucleation and growth of silica nanoparticles in alkaline condition that can be systematically transformed into hollow nanospheres (HSNs) as illustrated in Scheme 1. The initial droplets (~8 nm as observed in SAXS spectra) in reverse microemulsion are mainly water. The hydrophobic silica source TEOS dissolve in the oil phase of cyclohexane. The amphiphilic CA-520 and APTS reside mostly at the oil/water interface of the droplet. After NH₄OH was introduced into the reverse microemulsion, TEOS and APTS were catalytically hydrolyzed to form silanol groups (Si-O⁻ or Si-OH) and move into water droplet in the microemulsion and condensed into polymeric species.⁵³ After inter-droplet collision/exchange, the polysilicate species could initiate the nucleation of silica nanoparticle. Further growth of the surfactant-stabilized nuclei then occur through inter-droplet coalescence. Initially in the first 100 min, the sizes and SLD greatly fluctuated due to coexistence of different-diameter nanoparticles as they were just nucleated. However, after that nucleation was quenched, subsequent growth process become size-focusing as indicated by the reduced size variance in Fig. 4c.

3.5 The Effect of Chain Length of Alkanes: With the growth mechanism understood, we vary the oil phases in the reverse microemulsion systems which may impact the sizes of HSNs. Using alkanes of different chain lengths, e.g. *n*-hexane, *n*-octane, *n*-

decane, and *n*-dodecane as the continuous oil phase, we can create reverse microemulsion systems with different initial sizes. In all samples, a fixed amount of co-surfactant (*n*-hexanol, 2500 μ L) was added to stabilize microemulsion in these oil/surfactant systems. All experiments were also conducted with the same molar ratio of the oil component to the surfactant (CA-520). After the same growth process at 20 $^{\circ}$ C for 36 hours, the size of HSNs (from TEM images) synthesized from different oil are shown in Figure 7a-d and 7e. The average diameters of HSNs for products from *n*-hexane, *n*-octane, *n*-decane, and *n*-dodecane were determined as 42 ± 4 nm, 51 ± 6 nm, 60 ± 5 nm, and 71 ± 7 nm (Table S4). All the HSNs are very uniform in size with variance of size around 10%. Roughly speaking, a linear correlation between the HSN diameters and the solvent molar volume was found (Fig. 7e). The diameters of HSN became larger as chain-length of oil was increased. We also employed dynamic light scattering (DLS) to measure the microemulsion droplet sizes before introduction of TEOS or APTS. The size distributions of hydrodynamic diameters are shown in Figure S5. The w/o microemulsion system in *n*-hexane has shown the smallest droplet size among all oil phases. The hydrodynamic diameters of the w/o microemulsion droplets are positively correlated to the chain lengths of alkane. Previously, Zhao and coworkers reported a synthesis of silica nanoparticles using Triton X-100, with similar trend in tuning sizes using these alkanes.⁴⁰ Compared to Stöber silica, the size distributions here are broader which is due to the presence of APTS in our synthesis.³⁶ However, compared to silica hollow spheres reported in literature(except by hard templating), our HSNs are relatively uniform(less than 15% dispersity).

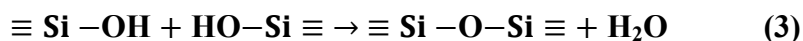
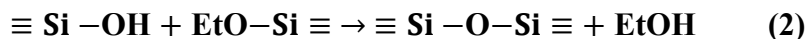
3.6 Effect of co-surfactant: It is known that the particle sizes synthesized in a microemulsion system are governed by the amount of cosurfactant besides the bulkiness of the oil molecule.²⁰ So, we investigate the effect of the co-surfactant (*n*-hexanol) on the diameters in HSN synthesis for the cyclohexane system. Here, we use the surfactant Triton X-100 instead of CA-520. Triton X-100 has longer hydrophilic groups than CA-520 while their hydrophobic groups are the same. To form stable microemulsion, a co-surfactant of more hydrophobic balance would be needed. The microemulsion system was composed of cyclohexane, water, Triton X-100, and *n*-hexanol. Without introducing *n*-hexanol in the system, the microemulsion could not be formed because the hydrophilic PEO group is too short and water and oil phases became immiscible. A co-surfactant, such as hexanol, is necessary to form microemulsion. After the same synthesis and etching process, the images and size distributions of HSNs are compared in Figure 8. Representative TEM images indicate that sizes of nanosphere and shell thicknesses increased with the amounts of *n*-hexanol added. A linear correlation of the final HSN diameters (60-170 nm in log scale) to the volumes of added *n*-hexanol was observed in Figure 8e and Fig. S6b. However, this diameter trend of *n*-hexanol added volume gives an opposite correlation to their initial microemulsion water droplet sizes. For example, adding 7 mL of *n*-hexanol into Triton X-100 system gives the smallest sized reverse micellar size in microemulsion but grows into the largest HSNs (175 nm)(Fig. S6). We note here that the co-surfactant *n*-hexanol behaves like surfactant in that an increasing of co-surfactant/surfactant would create more interfaces. Then more droplets of smaller size will be formed. However, the final increase of size of diameter of the resulting HSNs with respect to amount of

hexanol will be explained in section 4.2. To sum up, using *n*-hexanol as a co-surfactant to control the size of HSNs is a simple and effective method. The size of HSNs can be tuned from 60 nm to 170 nm as the added amount of *n*-hexanol is increased.

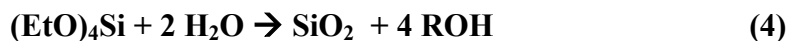
3.7 Effect of surfactant mixture: Finally, we examine the effect of mixing two surfactants. It has been observed that Triton X-100 can lead to HSNs with diameters larger than those made from CA-520. Therefore, one expects mixing these two surfactants may interpolate the diameters between HSNs made with a single surfactant. As shown in the TEM images in Figure 9, the size of the HSNs increased as relative molar ratio of Triton X-100 to CA-520 was increased. In addition, we observed significantly increased polydispersity in diameters when the percentage of Triton X-100 in the system was larger than 50%. The microemulsion behaviors in the mixing system do not follow a single size distribution, and the DLS analysis for the microemulsion in Figure S7 indicates a bimodal size distributions (5 nm and at 21 nm) of the water droplets before adding TEOS or APTS. But the final size distribution is still weakly bimodal. For example, when the percentage of Triton X-100 was 75%, the final SSN sizes were also redistributed into a bimodal profile having two centers around 60 and 90 nm.(Fig S7 inset) It clearly suggests that for this case the size-focusing effect is not strong enough to lead to mono-disperse distribution of the size of the final SSNs.

4. Discussion

In this section, we discuss the physical chemistry behind the growth process and the control of particle size of HSN in a reverse microemulsion. The chemical reactions involved in silica formation from TEOS, hydrolysis(Eq(1)) and condensation(Eq(2)(3)), as catalyzed by the highly alkaline ammonia solution, are



The net reaction is:



As the reactions proceed, TEOS consumes water and produces EtOH together with forming silanol and siloxane bonds. This makes the silicate species (oligomers) gradually move from the continuous phase to the water droplets where further condensation occurs. Meanwhile, the water droplet provides an environment similar to Stöber synthesis with a mixture of ammonia, water and ethanol solution. The droplet size grows initially as hydrolyzed silicates and APTS move into the water droplets. In fact, this can be regarded as a Stöber-like reaction occurred in a soft-confined space of nanoreactor. Then the silica nanoparticles grow by coalescence as silica condensation reaction takes over as the driving force for growth.

4.1 Evolution of Silica nanoparticles within Reverse Microemulsion: Here the role of microemulsion in synthesis of SSNs is examined to compare to the classical Stöber process. We focus on the evolution of size and SLD of the silica nanoparticles as depicted in Fig. 4c. In principle, there are three growth modes of nanoparticle:⁵⁴ e.g. classic (LaMer) nucleation and growth, aggregative growth, and Ostwald ripening. In

our system, the microemulsion droplets compartmented silicate species made the aggregation via inter-micellar contacts much slower compared to the corresponding Stöber process in homogeneous solution. The slowed-down kinetics allows us to observe in-situ the different stages in growth. Also, in microemulsion synthesis mass transfer of silica precursors via shrinkage and dissolution into oil phase is not effective. Ostwald ripening process, in our case, is not an important pathway in microemulsion synthesis at least initially.

Next, we examine the time evolution of diameter and SLD as we presented in Fig. 4c. In the beginning, one sees stage (1) at the first half hour where neither the SLD nor the size changed much. This is the induction period for nucleation.⁵⁵ There are hydrolysis reaction and solubilization going on, but little silica condensation occurred yet. We note here that previous time-evolution studies of Stöber process⁵⁶ did not identify any induction period because it was much faster in homogeneous solution compared to our reverse microemulsion system. In stage (2)(~30 to 100 min), one observed a rapid increase of SLD (Fig. 4a) which we interpret as the nucleation burst period. A LaMer nucleation/growth process and critical size aggregation result in a bimodal size distribution. In the same period, the mean particle diameter grows to about 18 nm but with a very large variance in size distribution at the end of nucleation period. This is reasonable since each particle will immediately grow after nucleated and this leads to big differences in sizes between particles that were nucleated at different time of the nucleation burst period. At the end of burst period, the size distribution is the broadest as we clearly see at the time of 100 min. Between 100 and 400 min (stage 3), the nucleation stopped and growth by diffusion/coalescence dominated. In the log-log plot

of Fig. 4c, one see a time dependence $\sim t^{1/2}$ (actual fit is $t^{0.48}$) which is characteristic of the classical Lifschitz-Slyozov(LS) for interface kinetic limited growth.⁵⁷ A supercritical silica particle grows by incorporating the silicate species in other reverse micelle (moving diffusively) after collision and fusion. In the final stage (4), the time evolution of diameter slowed down to a power law of $t^{0.21}$. The particle size is reaching a limiting value ~ 37 nm slowly. Because of this slow-down the size distribution is self-focusing and becomes narrower. This makes the reverse microemulsion method advantageous in size uniformity. According LS theory, if the growth is changed to diffusion-limited, the time evolution of diameter would be $t^{1/3}$ under unchanging concentration at infinite distance. Our observation of a slower growth law of $t^{0.21}$ may be due to the additional effect of a decreasing population of reverse micelles in solution.

Recently, in a detailed in-situ SAXS study of Stöber synthesis of silica nanoparticle, Tobler *et al.* found a 3-stage growth process⁵⁸: (1) nucleation of silica nanoparticles, (2) surface-controlled particle growth and (3) Ostwald ripening(OR) and particle aggregation. In our synthesis of silica nanoparticles, we found a first stage of induction period for nucleation event and surface-limited particle growth by fusing small reverse micelles. The surface-controlled growth by incorporating silicate-containing reverse micelles was evidenced by the $t^{1/2}$ dependence profile in our stage (2) and (3). However, unlike most solution synthesis of nanoparticles, the final stage of decreasing variance in size-distribution of our stage (4) makes the OR mechanism unlikely. Because of the compartmental effect of reverse micelles, Ostwald Ripening and aggregation are much reduced. Instead, we observed a final slow-down stage (4)

allowing a self-focusing effect of the size distribution of the product of silica nanoparticles.

4.2 The effects of changing continuum phase and interface composition:

The final diameters of silica nanoparticle are determined by coalescence kinetics of critical-size nanoparticles. We have seen that among the four stages of time evolution, the diffusive coalescence of micellar droplets (red line in Fig. 4c) dominated the growth process. Thus we have made changes in synthesis compositions in order to control the coalescence kinetics. Here we have reported three synthesis parameters on growing silica nanoparticles for different sizes: continuous phases, co-solvent amounts and surfactant mixture ratios.

In a reverse microemulsion system, the continuous phase (oil) interacts with hydrophobic parts of the surfactants, resulting in stable initial reverse micelles with well-defined sizes. In our microemulsion system, the polymeric surfactants wedge the micelles to lower the curvature. Thus, we examine the spontaneous curvature of the o/w interface when solvent is varied. In water/oil microemulsion, it has been reported that the radius of spontaneous curvature decreases as the chain length of oil decreases in an w/o microemulsion.⁵⁹ Indeed, we have measured by dynamical light scattering that the hydrodynamic diameter of w/o droplet decreases as the chain length becomes shorter, from 5.5 nm for n-hexane to 16 nm for n-dodecane [see Fig. S5]. The solvation of the hydrophobic polymeric chain of the surfactant CA-520 by the alkane solvent determine its effective size. A good solvent, such as hexane or cyclohexane, would swell the hydrophobic tails of the polymeric surfactant and gives higher curvature for the reverse micelle droplet. In contrast, a poor solvent, such as dodecane with a long

alkyl chain, would result in de-solvation and shrink of the hydrophobic tails. It then gives a lower curvature of the droplet.

When two droplets in a reverse microemulsion collide, they may fuse partially to establish fluid bridge and exchange contents and then separate. This coalescence is important when nucleated silica grows inside droplet. In addition to the attractive interaction due to dispersion force, short-range repulsive barrier to fusion is determined by the entropic force between interpenetrating polymer chains. An expanded polymeric configurations in good solvent would suffer more entropy loss when encounter each other upon collision of two interfaces and thus more resistant to fusion.⁶⁰ This then would give a stronger entropic repulsion between two approaching micelles which protects interface from fusion and coalescence. This would allow less fusion and coalescence of the two approaching interfaces. The result is a smaller silica nanoparticle when using good solvent as continuous phase in w/o microemulsion. In scheme 2, we depict the molecular interactions involved in coalescence process. The repulsive interaction between the reverse micelles, which gives rise to energy barrier against coalescence, is entropic in origin. This explains the trend of sizes for different chain lengths of alkane in Fig. 7e.

A second factor determining the energy barrier of fusion of droplets is the energy spend on forming Gaussian curvatures, e.g. saddle-shaped curvature. Here, the magnitude of saddle splay modulus κ' determines the corresponding energy.⁶¹ If κ' is positive and large, the saddle-like surfaces are favored with respect to planar. It has been long known adding a medium chain alcohol (such as hexanol) to a surfactant film normally increases the film flexibility for forming saddle-like shaped film.^{61, 62} The

presence of the cosurfactant hexanol decreases the strength of surfactant film and thus increases the fusion dynamics of micelles. This qualitative trend explains the results of increasing size with hexanol amount in Fig. 8e.

A third, though minor, factor in affecting the size of HSNs would be the partition equilibrium of hexanol between oil and micellar phases. Although partition of hexanol in micellar phase is favored, the large volume of oil phase makes the dissolution of hexanol in oil significant which decreases slowly with the chain length of alkanes.⁶³ So in heavier alkanes, there is more presence of hexanol in the oil-water interface. According to Fig. 9, this effect also tends to make the size of HSNs bigger for the higher alkanes. But this effect is relatively minor compared to the previous ones.

4.3 Why hollow structures are formed: We now discuss the process of forming hollow silica nanoparticle after repeated washing SSNs with warm water. Several etching methods of incompletely condensed silica nanoparticles to create internal voids or enlarged pores have been developed. In most literature reports, the etchings of silica are alkaline-based methods. However, for the very small silica nanoparticles alkaline-based etching method has been difficult to control. One needs an etching method that is mild and controllable. Yin and coworkers have recently reported warm water as etchant for making permeable silica nanoshells by surface-protected etching.⁶⁴ This process is particularly useful for treating small silica nanoparticles. It is expected that the etching efficiency is directly related to the degree of condensation of the silica network.

In our microemulsion-based synthesis, several factors lead to incomplete condensation of silica in the core region of silica nanoparticle. First, the PEO group in the polymeric surfactants stabilizes silica condensation in the interfacial region. Previously, Yin and coworkers⁶⁵ have used poly(vinyl pyrrolidone) (PVP) to stabilize the silica network structure in a “surface-protected etching” approach in making silica nanoshells. Either PVP or PEO can stabilize condensed silanol groups through hydrogen bonding interaction. This makes the shell region more condensed and less prone to etching. Secondly, ethanol solution of APTS was used in preparing the initial reaction solution which means that the continuous alkane phase is already saturated with ethanol in the beginning of synthesis. Thus, the production of EtOH in hydrolysis (eq(1)) and condensation (eq(2)) of TEOS and APTS has to stay inside the water pool. When enough EtOH is produced, it will shift the reactions to the left hand side of eq(1) and eq(2), e.g. less condensation of silicates. Thirdly, the use of APTS would lead to less silica condensation because it has one less condensable alkoxy group. However, from our leaching study, we found to our initial surprise that it is APTS preferentially stays on the silica nanoparticle upon etching with warm water. This is due to the self-catalysis activity of -NH_2 group in APTS for hydrolysis and condensation reaction (eq(1) and (2)).^{66, 67} Thus, APTS becomes more condensed than TEOS in the confined space of microemulsion. Putting together the above three factors, silica condensations of the silica source TEOS and APTS in the water pool of reverse microemulsion are less complete in the core region and lead to hollow silica nanosphere after etching with warm water.

5. Conclusion

In situ SAXS performs real-time monitoring for the formation of the ammonia-catalyzed silica nanoparticles in cyclohexane w/o microemulsion. Co-condensation of TEOS and APTS during the growth of silica creates an interesting system of partially condensed nanospheres that possess high negative potentials at pH=7. Etching with warm water of the silica nanoparticles then produced uniform hollow silica nanospheres. The diameters of the silica nanoparticles can be rationally controlled by changing oil phases, co-surfactants or mixing surfactant ratios. The diameter tuning range (20-160 nm) allows us to explore micelle growth pathway via aggregation and coalescence, where evolutions of both diameters and SLD values suggest sigmoidal-like growth kinetics. Upon detailed examination of the kinetics with in-situ SAXS, evolution of bimodal narrow distributions of the growing nanoparticles and a small constant-size water droplet could be followed in the aggregative coarsening behaviors in w/o microemulsion. We identify four stages of the evolution, induction, nucleation, diffusional growth and slow down. This allows one detailed knowledge for controlling the size and distribution of the hollow silica nanospheres.

ACKNOWLEDGMENT

We are grateful to National Synchrotron Radiation Research Center (Hsinchu, Taiwan) for supports in SAXS experiments and data analysis, National Taiwan University and Minister of Science and Technology (NSC-100-2120-M-002-011) for financial supports, Instrument Center of National Taiwan University for assistance in TEM and solid-state NMR experiments. .

ASSOCIATED CONTENT

Supporting Information: More characterizations (ξ -potential, SAXS fitting comparisons from Primus and IGOR, detail TEM and DLS results, elemental analysis and NMR calculations) and list tables for solvents, co-surfactants and surfactant ratios.

This material is available free of charge via the Internet at <http://pubs.acs.org>.

REFERENCES

1. J. Lee, J. C. Park and H. Song, *Adv. Mater.*, 2008, **20**, 1523-1528.
2. L. L. Li, F. Q. Tang, H. Y. Liu, T. L. Liu, N. J. Hao, D. Chen, X. Teng and J. Q. He, *ACS Nano*, 2010, **4**, 6874-6882.
3. J. Lian, Y. Xu, M. Lin and Y. T. Chan, *J. Am. Chem. Soc.*, 2012, **134**, 8754-8757.
4. J. Dou and H. C. Zeng, *J. Am. Chem. Soc.*, 2012, **134**, 16235-16246.
5. S. H. Wu, C. T. Tseng, Y. S. Lin, C. H. Lin, Y. Hung and C. Y. Mou, *J. Mater. Chem.*, 2011, **21**, 789-794.
6. C. H. Lin, X. Y. Liu, S. H. Wu, K. H. Liu and C. Y. Mou, *J. Phys. Chem. Lett.*, 2011, **2**, 2984-2988.
7. S. S. Cao, L. Fang, Z. Y. Zhao, Y. Ge, S. Piletsky and A. P. F. Turner, *Adv. Funct. Mater.*, 2013, **23**, 2162-2167.
8. F. P. Chang, Y. Hung, J. H. Chang, C. H. Lin and C. Y. Mou, *ACS Appl. Mater. Interfaces*, 2014, **6**, 6883-6890.
9. Y. S. Lin, S. H. Wu, C. T. Tseng, Y. Hung, C. Chang and C. Y. Mou, *Chem. Commun.*, 2009, 3542-3544.
10. S. Mohapatra, S. R. Rout, R. Narayan and T. K. Maiti, *Dalton Trans.*, 2014, **43**, 15841-15850.
11. M. Chen, L. Wu, S. Zhou and B. You, *Adv. Mater.*, 2006, **18**, 801-806.
12. W. J. Li, X. X. Sha, W. J. Dong and Z. C. Wang, *Chem. Commun.*, 2002, 2434-2435.
13. H. J. Hah, J. S. Kim, B. J. Jeon, S. M. Koo and Y. E. Lee, *Chem. Commun.*, 2003, 1712-1713.
14. H. P. Lin, Y. R. Cheng and C. Y. Mou, *Chem. Mater.*, 1998, **10**, 3772-+.
15. Y. Q. Yeh, B. C. Chen, H. P. Lin and C. Y. Tang, *Langmuir*, 2006, **22**, 6-9.
16. H. P. Hentze, S. R. Raghavan, C. A. McKelvey and E. W. Kaler, *Langmuir*, 2003, **19**, 1069-1074.
17. J. Yuan, X. T. Bai, M. W. Zhao and L. Q. Zheng, *Langmuir*, 2010, **26**, 11726-11731.
18. P. A. Williamson, P. J. Blower and M. A. Green, *Chem. Commun.*, 2011, **47**, 1568-1570.
19. S. P. Moulik and B. K. Paul, *Adv. Colloid. Interfac.*, 1998, **78**, 99-195.
20. L. Yang, R. S. Xie, L. Y. Liu, D. Q. Xiao and J. G. Zhu, *J. Phys. Chem. C*, 2011, **115**, 19507-19512.
21. V. Tchakalova, F. Testard, K. Wong, A. Parker, D. Benczedi and T. Zemb, *Colloids Surf., A*, 2008, **331**, 31-39.
22. X. J. Zhao, R. P. Bagwe and W. H. Tan, *Adv. Mater.*, 2004, **16**, 173-+.
23. S. Santra, R. P. Bagwe, D. Dutta, J. T. Stanley, G. A. Walter, W. Tan, B. M. Moudgil and R. A. Mericle, *Adv. Mater.*, 2005, **17**, 2165-2169.
24. F. J. Arriagada and K. Osseo-Asare, *J. Colloid Interface Sci.*, 1999, **211**, 210-220.
25. F. J. Arriagada and K. Osseo-Asare, *Colloids Surf., A*, 1999, **154**, 311-326.
26. H. M. Chen, T. Hu, X. M. Zhang, K. F. Huo, P. K. Chu and J. H. He, *Langmuir*, 2010, **26**, 13556-13563.
27. J. Wang, Z. H. Shah, S. Zhang and R. Lu, *Nanoscale*, 2014, **6**, 4418-4437.

28. J. Eastoe, M. J. Hollamby and L. Hudson, *Adv. Colloid Interface Sci.*, 2006, **128-130**, 5-15.
29. A. K. Ganguli, A. Ganguly and S. Vaidya, *Chem. Soc. Rev.*, 2010, **39**, 474-485.
30. Y. H. Jin, A. Z. Li, S. G. Hazelton, S. Liang, C. L. John, P. D. Selid, D. T. Pierce and J. X. Zhao, *Coord. Chem. Rev.*, 2009, **253**, 2998-3014.
31. J. N. Park, A. J. Forman, W. Tang, J. H. Cheng, Y. S. Hu, H. F. Lin and E. W. McFarland, *Small*, 2008, **4**, 1694-1697.
32. C. W. Lu, Y. Hung, J. K. Hsiao, M. Yao, T. H. Chung, Y. S. Lin, S. H. Wu, S. C. Hsu, H. M. Liu, C. Y. Mou, C. S. Yang, D. M. Huang and Y. C. Chen, *Nano Lett.*, 2007, **7**, 149-154.
33. A. F. Zhang, Y. C. Zhang, N. Xing, K. K. Hou and X. W. Guo, *Chem. Mater.*, 2009, **21**, 4122-4126.
34. S. J. Park, Y. J. Kim and S. J. Park, *Langmuir*, 2008, **24**, 12134-12137.
35. S. Shi, M. Wang, C. Chen, F. Lu, X. Zheng, J. Gao and J. Xu, *Rsc Adv.*, 2013, **3**, 1158-1164.
36. F. P. Chang, Y. P. Chen and C. Y. Mou, *Small*, 2014, **10**, 4785-4795.
37. Z. Jin, F. Wang, F. Wang, J. X. Wang, J. C. Yu and J. F. Wang, *Adv. Funct. Mater.*, 2013, **23**, 2137-2144.
38. Z. G. Teng, X. D. Su, Y. Y. Zheng, J. Sun, G. T. Chen, C. C. Tian, J. D. Wang, H. Li, Y. N. Zhao and G. M. Lu, *Chem. Mater.*, 2013, **25**, 98-105.
39. X. L. Fang, Z. H. Liu, M. F. Hsieh, M. Chen, P. X. Liu, C. Chen and N. F. Zheng, *ACS Nano*, 2012, **6**, 4434-4444.
40. Y. H. Jin, S. Lohstreter, D. T. Pierce, J. Parisien, M. Wu, C. Hall and J. X. J. Zhao, *Chem. Mater.*, 2008, **20**, 4411-4419.
41. F. Asaro, A. Benedetti, N. Savko and G. Pellizer, *Langmuir*, 2009, **25**, 3224-3231.
42. P. Riello, M. Mattiazzi, J. S. Pedersen and A. Benedetti, *Langmuir*, 2008, **24**, 5225-5228.
43. F. Asaro, A. Benedetti, I. Freris, P. Riello and N. Savko, *Langmuir*, 2010, **26**, 12917-12925.
44. K. S. Finnie, J. R. Bartlett, C. J. A. Barbe and L. G. Kong, *Langmuir*, 2007, **23**, 3017-3024.
45. D. Langevin, *Annu. Rev. Phys. Chem.*, 1992, **43**, 341-369.
46. A. Gutierrez-Becerra, M. Barcena-Soto, V. Soto, J. Arellano-Ceja, N. Casillas, S. Prevost, L. Noirez, M. Gradzielski and J. I. Escalante, *Nanoscale Res. Lett.*, 2012, **7**, 1-12.
47. P. Podsiadlo, S. G. Kwon, B. Koo, B. Lee, V. B. Prakapenka, P. Dera, K. K. Zhuravlev, G. Krylova and E. V. Shevchenko, *J. Am. Chem. Soc.*, 2013, **135**, 2435-2438.
48. Y. Chen, P. Xu, H. Chen, Y. Li, W. Bu, Z. Shu, Y. Li, J. Zhang, L. Zhang, L. Pan, X. Cui, Z. Hua, J. Wang, L. Zhang and J. Shi, *Adv. Mater.*, 2013, **25**, 3100-3105.
49. R. M. Anisur, J. Shin, H. H. Choi, K. M. Yeo, E. J. Kang and I. S. Lee, *J. Mater. Chem.*, 2010, **20**, 10615-10621.
50. Q. W. Shanshan Li, Zonghua Qin, Yuhong Fu, and Yuantao Gu, *Langmuir*, 2015, **31**, 824-832.
51. C.-L. Chang and H. S. Fogler, *Langmuir*, 1997, **13**, 3295-3307.
52. V. F. Sears, *Neutron News*, 1992, **3**, 26-37.

53. C. L. Chang and H. S. Fogler, *AIChE J.*, 1996, **42**, 3153-3163.
54. F. D. Wang, V. N. Richards, S. P. Shields and W. E. Buhro, *Chem. Mater.*, 2014, **26**, 5-21.
55. S. J. D.L Green, Yui-Fai Lam, M.T Harrisa,, *J. Non-Cryst. Solids*, 2003, **315**, 166-179.
56. D. Pontoni, T. Narayanan and A. R. Rennie, *Langmuir*, 2002, **18**, 56-59.
57. I. M. Lifshitz and V. V. Slyozov, *J. Phys. Chem. Solids*, 1961, **19**, 35-50.
58. D. J. Tobler, S. Shaw and L. G. Benning, *Geochim. Cosmochim. Acta*, 2009, **73**, 5377-5393.
59. M. J. Hou and D. O. Shah, *Langmuir*, 1987, **3**, 1086-1096.
60. B. Lemaire, P. Bothorel and D. Roux, *J. Phys. Chem.*, 1983, **87**, 1023-1028.
61. A. Kabalnov, B. Lindman, U. Olsson, L. Piculell, K. Thuresson and H. Wennerström, *Colloid. Polym. Sci.*, 1996, **274**, 297-308.
62. P. G. T. De Gennes, C., *J. Phys. Chem.* , 1982, **86**, 2294-2304.
63. R. Aveyard and R. W. Mitchell, *Trans. Faraday Soc.*, 1969, **65**, 2645-&.
64. Y. X. Hu, Q. Zhang, J. Goebel, T. R. Zhang and Y. D. Yin, *PCCP*, 2010, **12**, 11836-11842.
65. Q. Zhang, T. R. Zhang, J. P. Ge and Y. D. Yin, *Nano Lett.*, 2008, **8**, 2867-2871.
66. I. A. Rahman, M. Jafarzadeh and C. S. Sipaut, *Ceram. Int.*, 2009, **35**, 1883-1888.
67. A. van Blaaderen and A. Vrij, *J. Colloid Interface Sci.*, 1993, **156**, 1-18.

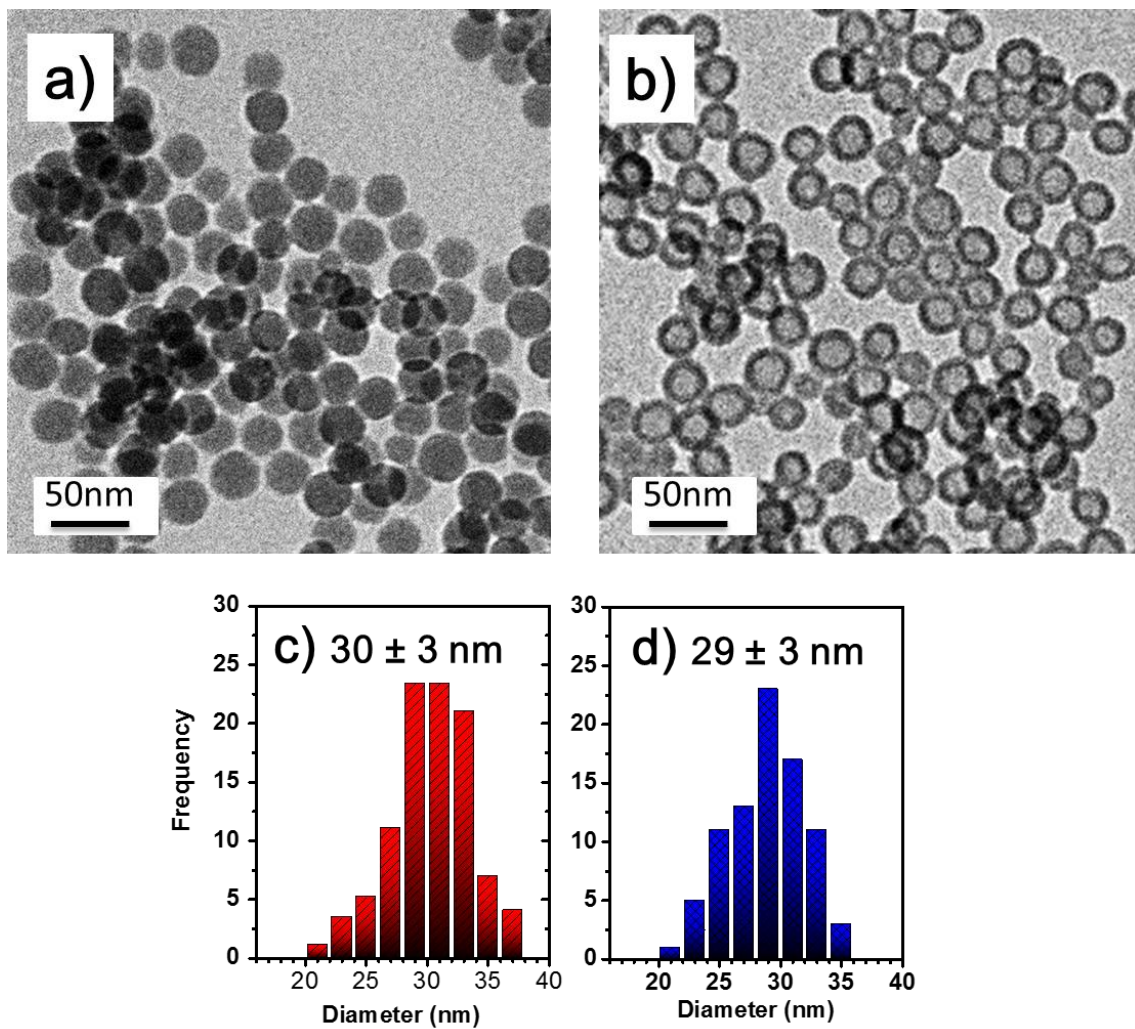


Figure 1. Representative TEM images and size distribution analysis of the un-etched solid silica nanoparticles (SSNs)(a,c) and hollow silica nanospheres (HSNs)(b,d).

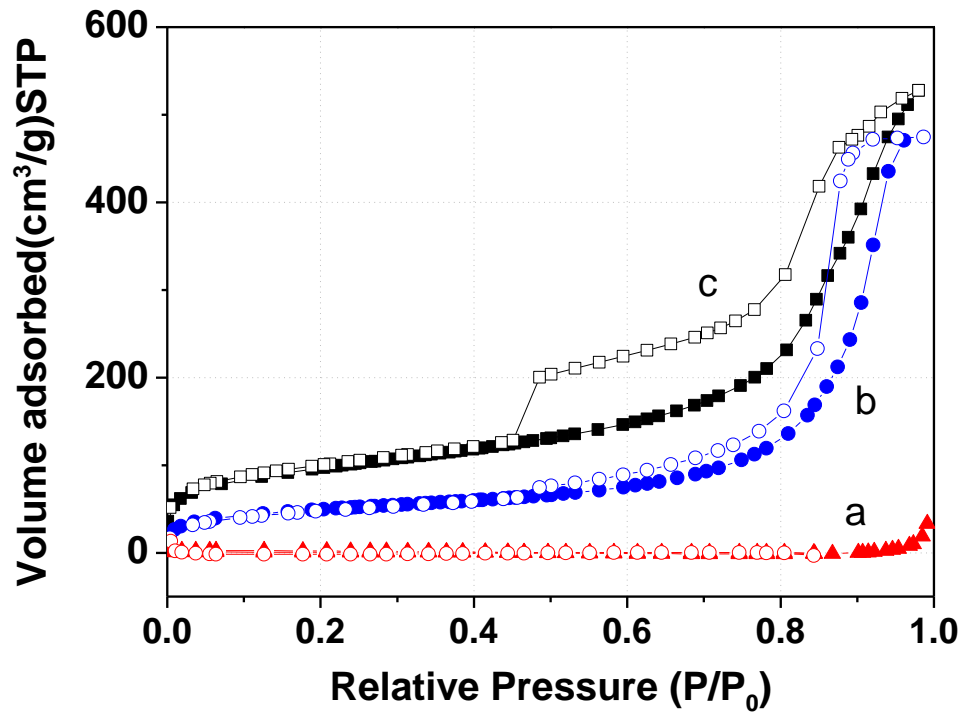


Figure 2. N₂ adsorption-desorption isotherms of (a) SSN (red symbol-curves), (b) as-prepared HSNs after warm-solution washing (blue symbol-curves) and (c) HSNs after calcination at 560 °C (black-symbol curves).

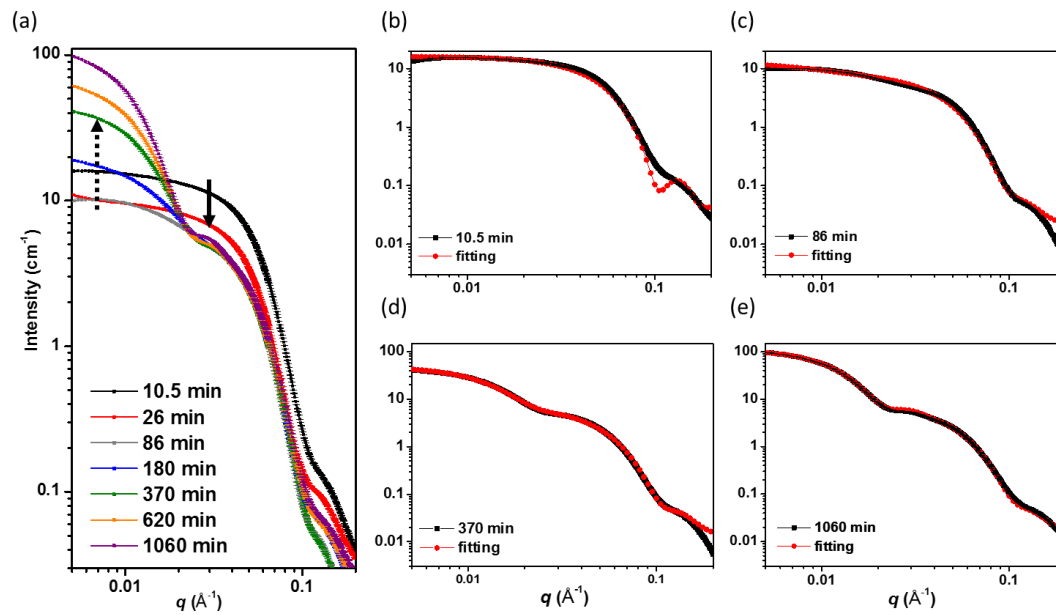


Figure 3. (a) All SAXS experimental (dot-curve) and selected fitting results (red dot-curve) from bimodal spheres in Schulz size distribution function for SSN growth reaction after (b) 10.5 min, (c) 86 min, (d) 370min, and (e) 1060 min.

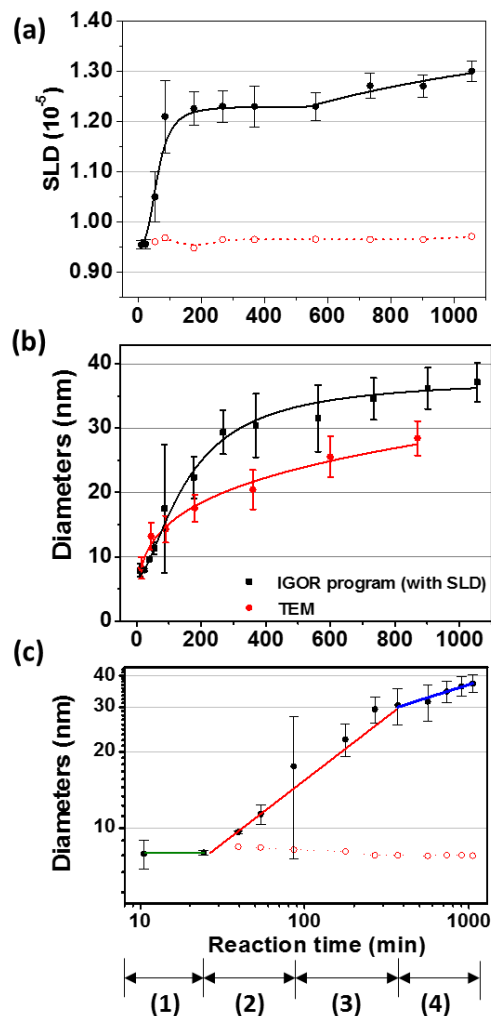


Figure 4. (a) SLD calculations and (b) diameters of solid silica nanoparticles (●) and reverse microemulsion (○) via bimodal spheres in Schulz size distribution function with polydispersity parameters for diameter uncertainty. (c) Stages of the size evolution for SSN growth as denoted under X-axis: (1) induction period, (2) nucleation burst, (3) growth by diffusion-coalescence, (4) slowdown of growth stage.

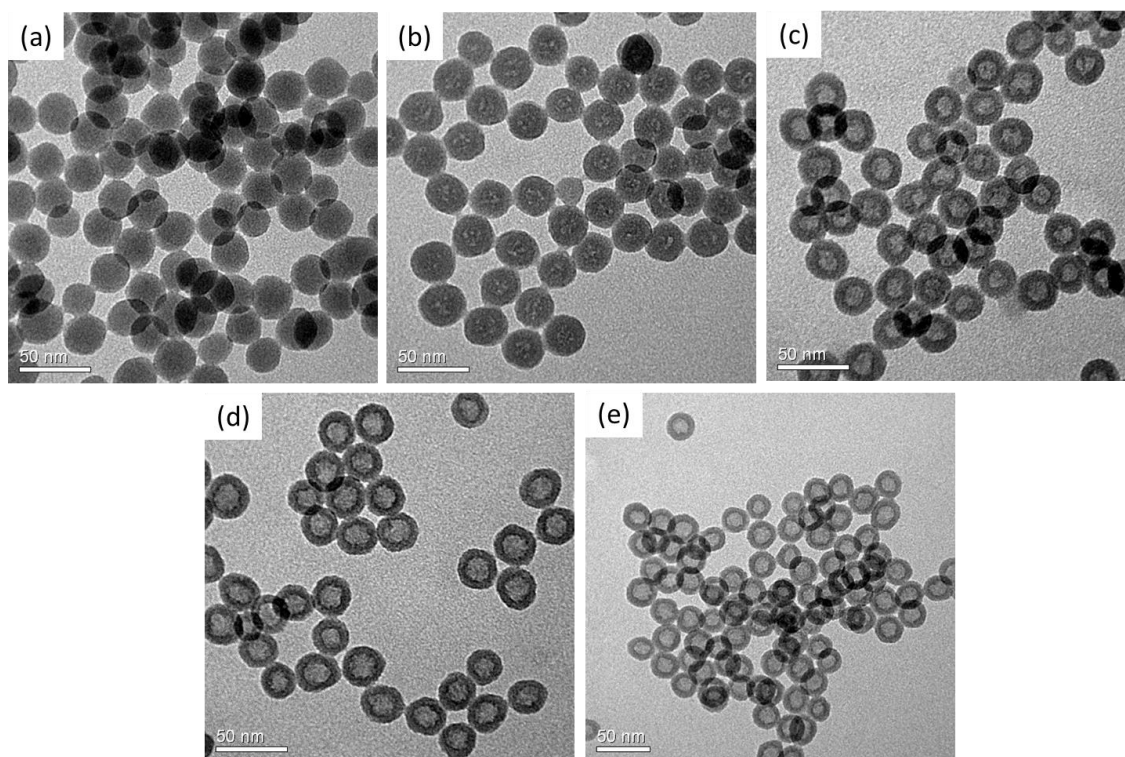


Figure 5. The etching process of HSN at (a) 0 min (b) 10 min (c) 20 min (d) 30 min (e) 40 min

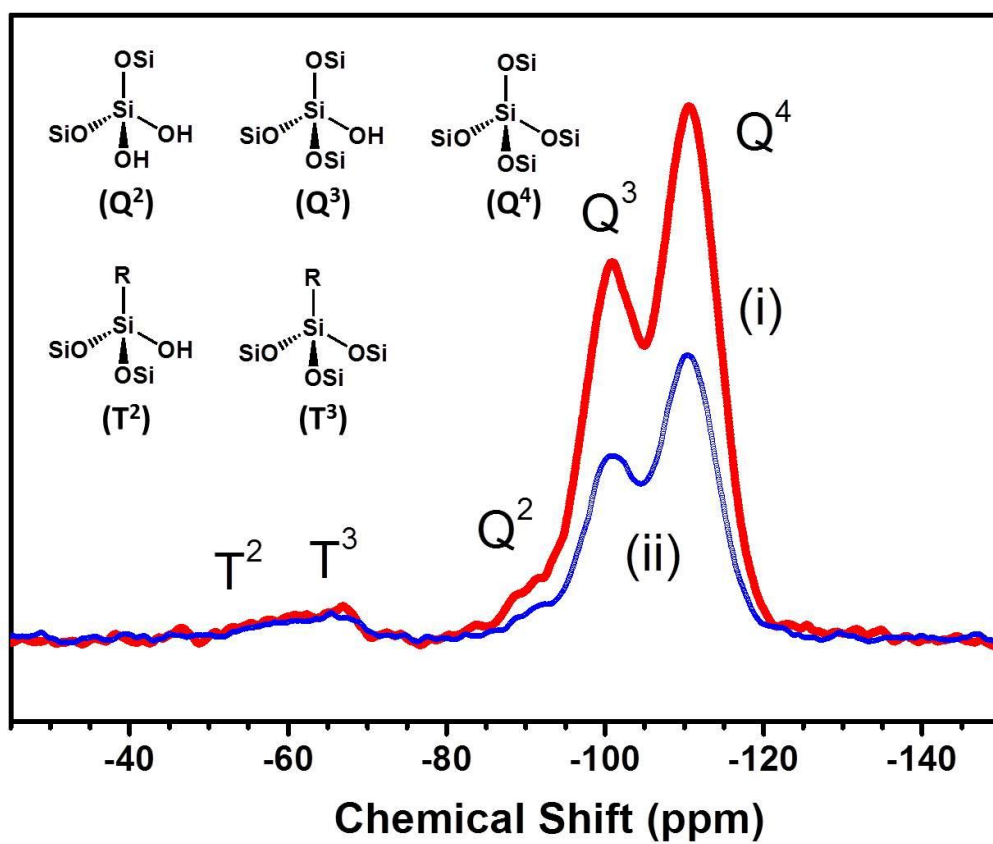


Figure 6. (a) ^{29}Si solid-state NMR spectra of SSNs (i, red curve) and HSNs (ii, blue curve).

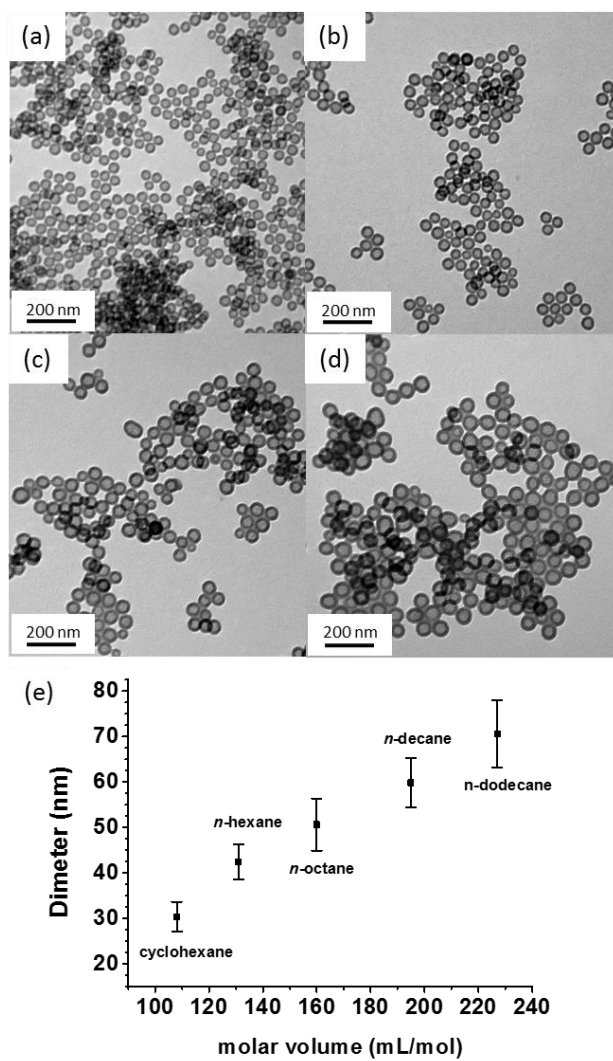


Figure 7. Representative TEM images for HSNs synthesized in various alkyl-chain solvent systems: (a) *n*-hexane, (b) *n*-octane, (c) *n*-decane, (d) *n*-dodecane. The size distributions and their correlations to the solvent molar volumes are plotted in (e).

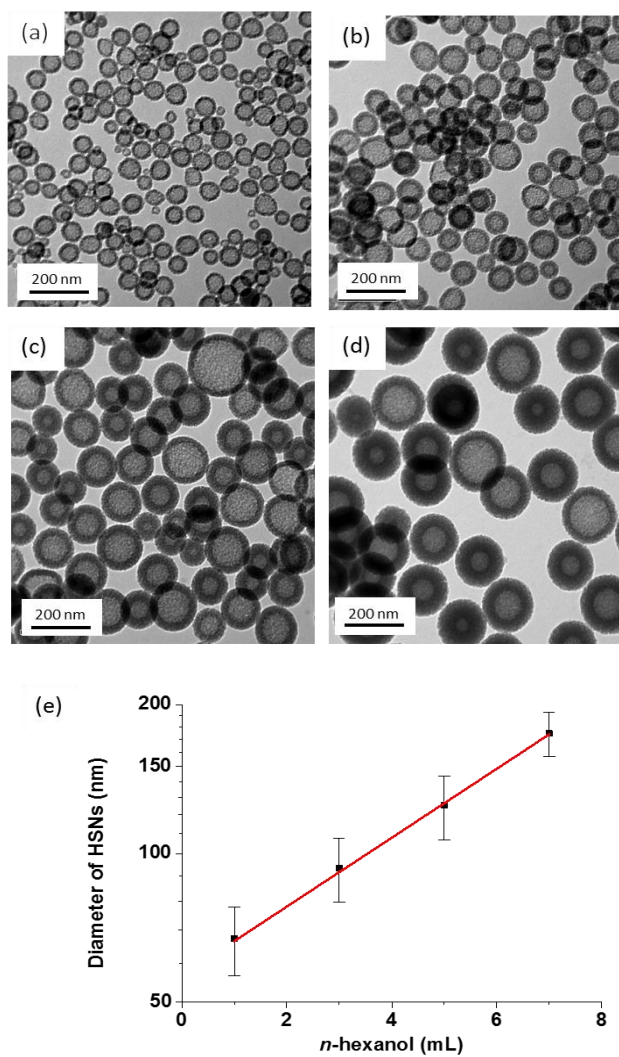


Figure 8. TEM images and size distribution of HSNs synthesized in the cyclohexane system with different volume of *n*-hexanol: (a) 1 mL, (b) 3 mL, (c) 5 mL, (d) 7 mL. (e) A relationship between the different volume of *n*-hexanol added and the corresponding diameters (in log scale) of the HSNs.

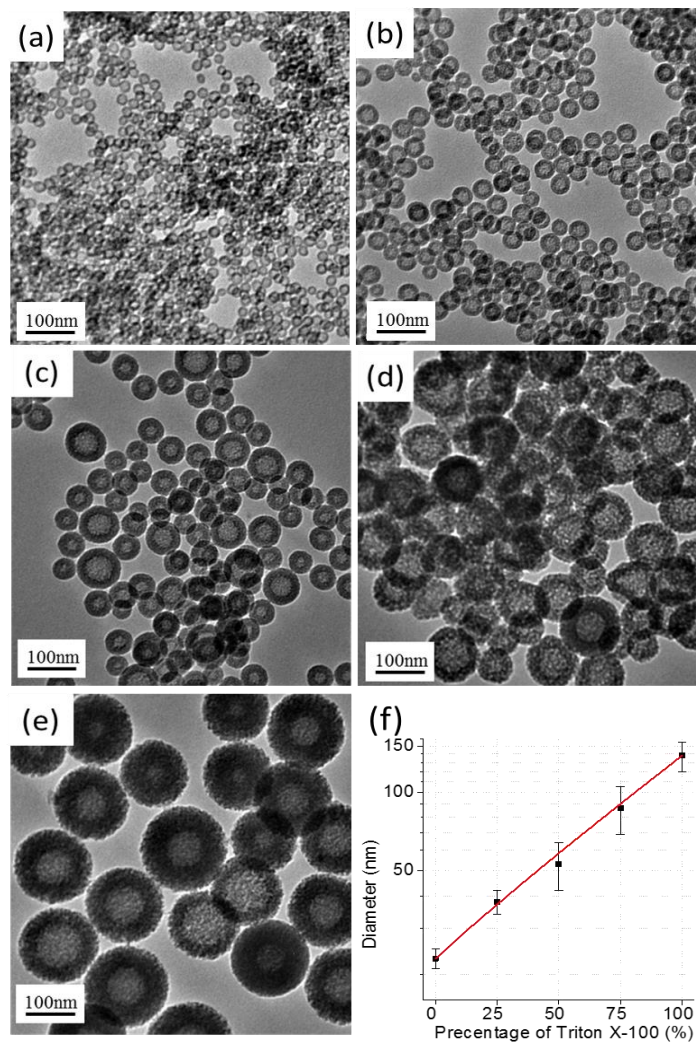
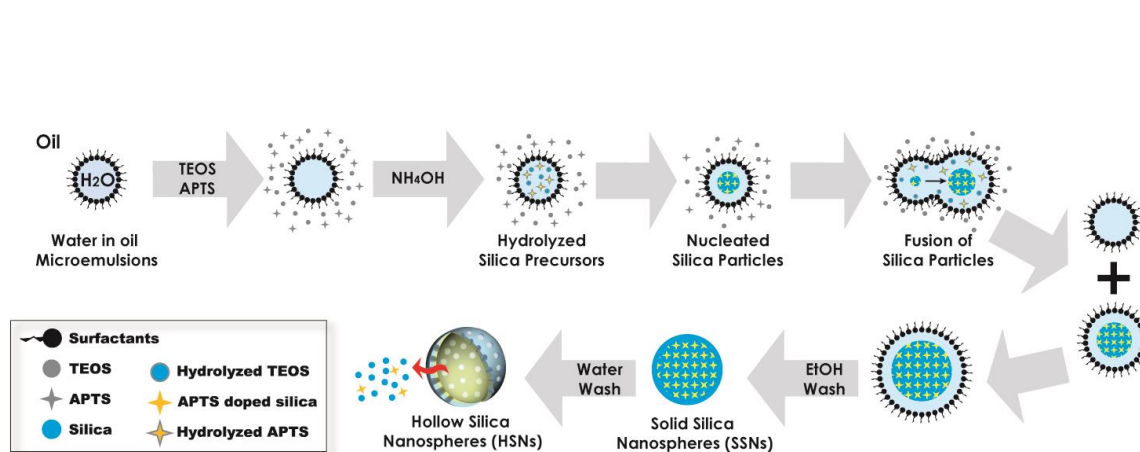
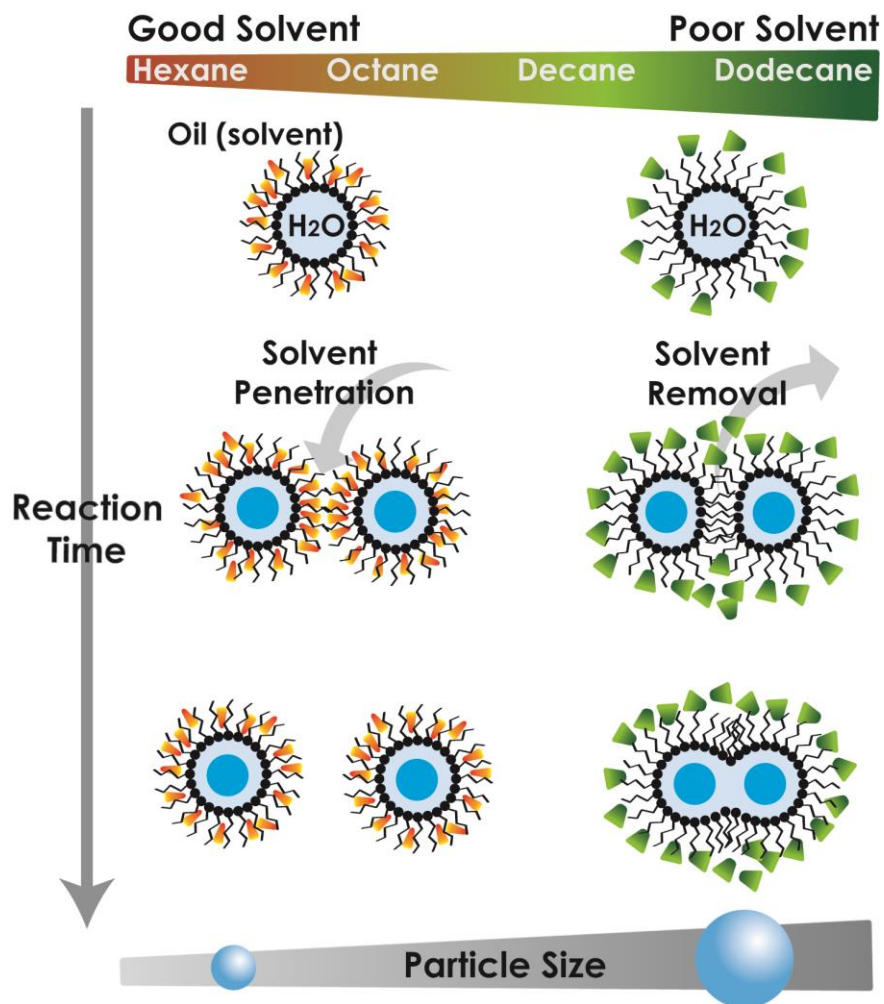


Figure 9. Representative TEM images of HSNs synthesized with various amounts of (a) 0, (b) 25%, (c) 50%, (d) 75% and (e) 100% Triton X-100 over CA-520. (f) Correlation of Triton X-100 molar ratio (%) to HSNs' diameters (in log scale).



Scheme 1. The nucleation and growth mechanism of silica nanoparticles and nanospheres.



Scheme 2. Solvent-initiated fusion pathways for silica nanoparticle formation. The fusion tendency of droplets in w/o microemulsion is primarily determined by solvent compatibility with the hydrophobic chain as varied in chain length of the continuous phase (oil).

Table 1. Textural properties of SSN, HSN and calcined HSN determined by N₂ adsorption isotherms.

	BET surface area (m²/g)	Pore volume (cm³/g)	<u>Micropore</u> surface area (t-plot, m²/g)
SSN	6.09	0.05	6.09
HSN	170.74	0.72	53.66
<u>Calcined HSN</u>	359.14	1.09	206.35